Dynamical Properties of Two Semiconductor Lasers with Bidirectional Optoelectronic Coupling

Raúl Vicente[a], Josep Mulet[a], Claudio R. Mirasso[a], Shuo Tang[b] and Jia-ming Liu[b]

[a]Departament de Física, Universitat de les Illes Balears, Campus UIB, E-07071 Palma de Mallorca, Spain

[b]Department of Electrical Engineering, University of California at Los Angeles, Los Angeles, California 90095-159410 USA

ABSTRACT

We have studied the dynamical behaviour of two semiconductor lasers subject to an optoelectronic bidirectional coupling and optionally to feedback, considering non-zero delay times in the propagation of the signals between both lasers and through each feedback loop in the case the latter exists. Starting from delayed rate equations for the photon and carrier densities, we have investigated the stability of the fixed points and limit cycles of the system as function of the coupling and feedback strengths, as well as the delay times. From this analysis, quasiperiodic route to chaos and several interesting phenomena like the recently discovered "death by delay" are predicted for this system.

Keywords: Semiconductor Lasers, Delay, Instabilities in Diode Lasers, Bidirectional Coupling.

1. INTRODUCTION

Neurons, chemical oscillators, Josephson junctions or semiconductor lasers are just a few examples of nonlinear systems, whose connection or coupling with similar units can lead to a very rich dynamics. Their importance in both theoretical and practical applications has concentrated great attention of the researchers into the study of such systems for a long time. However, it is only recent the interest in considering the effects of time delayed connections which arise naturally when the finite speed of propagation of signals is taken into account. The inclusion of these delay times in a given model not only introduces an infinite dimensional phase space[1] but also provides a new source of possible instabilities. In this direction, special attention has been captured by the recently discovered phenomenon denominated "death by delay"[2–5] by which oscillation death of two coupled limit cycle oscillators is induced by the time delay in the coupling. In section 4.2 a new observation of this phenomenon for the system under study is reported.

Impelled by the curiosity to know the role of different delay times in semiconductor lasers, in this work we have studied the configuration of two semiconductor lasers subject to optoelectronic bidirectional coupling with and without a feedback loop for each of them. Former studies have dealt with the case of isolated lasers subject to optoelectronic feedback[6–10] or with unidirectional coupling schemes,[11,12] reporting several interesting dynamical regimes like anticipating and retarded synchronization but to our best knowledgement no one has investigated the dynamical properties of the system under study. The choice of the optoelectronic case allows to a deeper understanding than other situations since we avoid the complexity introduced by the phase of the electrical field whose dynamics can be decoupled from the rest of variables unlike the coherent optical case in which it plays a major role.[13,14]

For our study two configurations have been considered depending on both lasers or neither of them is subject to the optoelectronic feedback. In all cases bidirectional optoelectronic coupling is present.

This work is divided as follows. In Section 2 we present the modeling of the system that is performed at the level of modified rate equations. In the next two sections, the fixed points and limit cycles of the system as

Telephone: 34-971172505, Fax: 34-971173426, http://www.imedea.uib.es/Photonics,
E-mail address: raulv@imedea.uib.es

well as their stability are investigated. In the same section some codimension one and two bifurcations are illustrated together the analysis of the route to chaos followed by the system when the delay time is varied. The observation of the "death by delay" while increasing the coupling time when both lasers are self-pulsating due to the feedback is also reported there. Finally, future directions and conclusions are given in Section 5.

2. THE MODEL

We consider the system depicted in Figure 1, where the optical power output emerging from each one of the lasers is converted in electrical current and after an amplification process it is added to the bias current of the other laser (optoelectronic coupling) and to its own injection current (optoelectronic feedback).

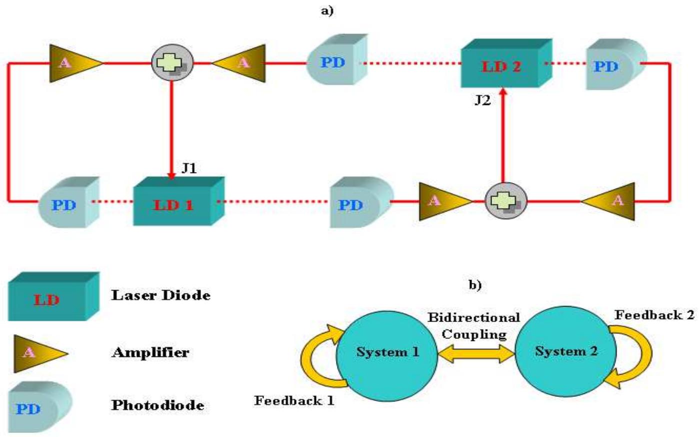

Figure 1. a) Scheme for two lasers with optoelectronic bidirectional coupling and feedback. b) Topology of the connections.

The equations used to model this system correspond to the usual single-mode semiconductor laser rate equations modified by the presence of a delay term of the optical power of each laser into the population inversion of the other one (optoelectronic coupling) and into its own population inversion (optoelectronic feedback). Then, the rate equations for the evolution of the photon and carrier densities read[10]

$$\frac{dS_1}{dt} = -\gamma_{c_1} S_1 + \Gamma g_1 S_1 \tag{1}$$
$$\frac{dN_1}{dt} = \frac{J_1}{ed} + \xi_{f_1} S_1(t-\tau_{f1}) + \xi_{c_1} S_2(t-\tau_{c1}) - \gamma_{s_1} N_1 - g_1 S_1 \tag{2}$$

$$\frac{dS_2}{dt} = -\gamma_{c_2} S_2 + \Gamma g_2 S_2 \tag{3}$$
$$\frac{dN_2}{dt} = \frac{J_2}{ed} + \xi_{f_2} S_2(t-\tau_{f2}) + \xi_{c_2} S_1(t-\tau_{c2}) - \gamma_{s_2} N_2 - g_2 S_2 \tag{4}$$

where S is the intracavity photon density, N is the carrier density, g is the optical gain coefficient, ξ_c (ξ_f) is the coupling (feedback) parameter which corresponds to the strength of the coupling (feedback) and τ_c (τ_f) is the coupling (feedback) delay time.

Other parameters appearing in the rate equations are the bias current density J, the inverse cavity photon lifetime γ_c, the inverse carrier lifetime γ_s, the confinement factor of the laser waveguide Γ, the electron charge

e and the active layer thickness d. The subindex (1 or 2) distinguishes between both lasers. Phase dynamics do not enter here because of the insensitivity of the photodetector to the phase of the electrical field.

Numerically calculated gains and also experimental results show that in a very wide range the optical gain coefficient has a linear dependence in both the carrier and photon density. Therefore, $g(N, S)$ is expanded as

$$g \approx g_0 + g_n(N - N_0) + g_p(S - S_0) \tag{5}$$

where $g_0 = \gamma_c/\Gamma$ is the gain coefficient at free-running condition, $g_n = \partial g/\partial N > 0$ is the differential gain parameter, $g_p = \partial g/\partial S < 0$ is the nonlinear gain parameter, N_0 is the carrier density at threshold and S_0 is the free-running intracavity photon density when the laser is not subject to either feedback nor coupling. Over a large range of operation the parameters g_n and g_p can be considered quite accurately as constants.

After introducing (5) into equations (1-4) and defining the dimensionless variables $\bar{s} \equiv (S - S_0)/S_0$, $\bar{n} \equiv (N - N_0)/N_0$, $\bar{J} = (J/ed - \gamma_s N_0)/\gamma_s N_0$, $\bar{\xi}_c \equiv \xi_c \Gamma/\gamma_c$ and $\bar{\xi}_f \equiv \xi_f \Gamma/\gamma_c$, the rate equations read

$$\frac{d\bar{s}_1}{dt} = \frac{\gamma_{c_1}\gamma_{n_1}}{\gamma_{s_1}\bar{J}_1}\bar{n}_1(\bar{s}_1 + 1) - \gamma_{p_1}\bar{s}_1(\bar{s}_1 + 1) \tag{6}$$

$$\begin{aligned} \frac{d\bar{n}_1}{dt} &= \gamma_{s_1}\bar{\xi}_{f_1}\bar{J}_1\left[1 + \bar{s}_1(t - \tau_{f_1})\right] + \gamma_{s_1}\bar{\xi}_{c_1}\bar{J}_1\left[1 + \bar{s}_2(t - \tau_{c_1})\right] \\ &\quad - \gamma_{s_1}\bar{n}_1 - \gamma_{s_1}\bar{J}_1\bar{s}_1 - \gamma_{n_1}\bar{n}_1(1 + \bar{s}_1) + \frac{\gamma_{s_1}\gamma_{p_1}}{\gamma_{c_1}}\bar{J}_1\bar{s}_1(1 + \bar{s}_1) \end{aligned} \tag{7}$$

$$\frac{d\bar{s}_2}{dt} = \frac{\gamma_{c_2}\gamma_{n_2}}{\gamma_{s_2}\bar{J}_2}\bar{n}_2(\bar{s}_2 + 1) - \gamma_{p_2}\bar{s}_2(\bar{s}_2 + 1) \tag{8}$$

$$\begin{aligned} \frac{d\bar{n}_2}{dt} &= \gamma_{s_2}\bar{\xi}_{f_2}\bar{J}_2\left[1 + \bar{s}_2(t - \tau_{f_2})\right] + \gamma_{s_2}\bar{\xi}_{c_2}\bar{J}_2\left[1 + \bar{s}_1(t - \tau_{c_2})\right] \\ &\quad - \gamma_{s_2}\bar{n}_2 - \gamma_{s_2}\bar{J}_2\bar{s}_2 - \gamma_{n_2}\bar{n}_2(1 + \bar{s}_2) + \frac{\gamma_{s_2}\gamma_{p_2}}{\gamma_{c_2}}\bar{J}_2\bar{s}_2(1 + \bar{s}_2) \end{aligned} \tag{9}$$

where the differential and nonlinear carrier relaxation rates are defined as $\gamma_n \equiv g_n S_0$ and $\gamma_p \equiv -\Gamma g_p S_0$, respectively. It is worth noting that since $S_0 = \bar{J}\gamma_s N_0 \Gamma/\gamma_c$, both γ_n and γ_p are related to the bias current.

The adimensional coupling (feedback) strength can be easily related to the responsivity of the corresponding photodiode and the amplification factor a of the associated amplifier in the following way

$$\bar{\xi} = a\frac{\eta c \alpha_m \Gamma}{2 n_g \gamma_c}\eta_{ext} \tag{10}$$

where η is the quantum efficiency of the photodetector, η_{ext} is a parameter that takes into account additional external losses, c is the speed of light in vacuum, α_m are the facet losses and n_g is the group refractive index. For a typical case ($\eta = 0.5$, $\eta_{ext} = 1$, $\alpha_m = 48$ cm^{-1}, $n_g = 3.5$, $\gamma_c = 0.24$ ps^{-1} and $\Gamma = 0.3$) $\bar{\xi}$ takes the value 0.13, when a has been fixed to one. Then, the magnitude of $\bar{\xi}$ can be easily modified just by changing the value of the amplification factor. In addition, the sign of $\bar{\xi}$ can be reversed substracting the generated photocurrent from the bias instead of add to it. In this work we consider both positive and negative values for the coupling and feedback strength.

For convenience, in the following we will drop the bars over the variables and parameters, understanding that they should not be confused with the original ones.

3. FIXED POINTS

The fixed points of the system (6-9) are obtained by imposing the conditions $s_1(t) = s_{1st}$, $s_2(t) = s_{2st}$, $n_1(t) = n_{1st}$ and $n_2(t) = n_{2st}$. Since we are interested in determining the effect of the different delay times and strengths on the dynamics of the system, we simplify our analysis considering the case of identical bias currents (ie., $J_1 = J_2 = J$) and internal parameters for both lasers. Now, it can be easily determined the existence of four fixed points which read

$$\left.\begin{array}{l}
s_{1st} = \dfrac{\gamma_c\,\gamma_n\left(\left(-\xi_{c_1}-\xi_{c_1}\,\xi_{c_2}-\xi_{f_1}+\xi_{f_1}\,\xi_{f_2}\right)\gamma_c\,\gamma_n-\left(\xi_{c_1}+\xi_{f_1}\right)\gamma_p\,\gamma_s\right)}{\left(-1+\xi_{c_1}\,\xi_{c_2}+\xi_{f_1}+\xi_{f_2}-\xi_{f_1}\,\xi_{f_2}\right)\gamma_c{}^2\,\gamma_n{}^2+\left(-2+\xi_{f_1}+\xi_{f_2}\right)\gamma_c\,\gamma_n\,\gamma_p\,\gamma_s-\gamma_p{}^2\,\gamma_s{}^2} \\
n_{1st} = \dfrac{\gamma_p\,\gamma_s\left(\left(-\xi_{c_1}-\xi_{c_1}\,\xi_{c_2}-\xi_{f_1}+\xi_{f_1}\,\xi_{f_2}\right)\gamma_c\,\gamma_n-\left(\xi_{c_1}+\xi_{f_1}\right)\gamma_p\,\gamma_s\right)J}{\left(-1+\xi_{c_1}\,\xi_{c_2}+\xi_{f_1}+\xi_{f_2}-\xi_{f_1}\,\xi_{f_2}\right)\gamma_c{}^2\,\gamma_n{}^2+\left(-2+\xi_{f_1}+\xi_{f_2}\right)\gamma_c\,\gamma_n\,\gamma_p\,\gamma_s-\gamma_p{}^2\,\gamma_s{}^2} \\
s_{2st} = \dfrac{\gamma_c\,\gamma_n\left(\left(-\xi_{c_2}-\xi_{c_1}\,\xi_{c_2}-\xi_{f_2}+\xi_{f_1}\,\xi_{f_2}\right)\gamma_c\,\gamma_n-\left(\xi_{c_2}+\xi_{f_2}\right)\gamma_p\,\gamma_s\right)}{\left(-1+\xi_{c_1}\,\xi_{c_2}+\xi_{f_1}+\xi_{f_2}-\xi_{f_1}\,\xi_{f_2}\right)\gamma_c{}^2\,\gamma_n{}^2+\left(-2+\xi_{f_1}+\xi_{f_2}\right)\gamma_c\,\gamma_n\,\gamma_p\,\gamma_s-\gamma_p{}^2\,\gamma_s{}^2} \\
n_{2st} = \dfrac{\gamma_p\,\gamma_s\left(\left(-\xi_{c_2}-\xi_{c_1}\,\xi_{c_2}-\xi_{f_2}+\xi_{f_1}\,\xi_{f_2}\right)\gamma_c\,\gamma_n-\left(\xi_{c_2}+\xi_{f_2}\right)\gamma_p\,\gamma_s\right)J}{\left(-1+\xi_{c_1}\,\xi_{c_2}+\xi_{f_1}+\xi_{f_2}-\xi_{f_1}\,\xi_{f_2}\right)\gamma_c{}^2\,\gamma_n{}^2+\left(-2+\xi_{f_1}+\xi_{f_2}\right)\gamma_c\,\gamma_n\,\gamma_p\,\gamma_s-\gamma_p{}^2\,\gamma_s{}^2}
\end{array}\right\}\text{F.P. I} \tag{11}$$

defining a fixed point in which both lasers are lasing,

$$\left.\begin{array}{r}
s_{1st} = -1 \\
n_{1st} = J \\
s_{2st} = -1 \\
n_{2st} = J
\end{array}\right\}\text{F.P. II} \tag{12}$$

which stands for the off-state, and finally

$$\left.\begin{array}{r}
s_{1st} = \dfrac{\xi_{f_1}\,\gamma_c\,\gamma_n}{\gamma_c\left(\gamma_n-\xi_{f_1}\,\gamma_n\right)+\gamma_p\,\gamma_s} \\
n_{1st} = \dfrac{\xi_{f_1}\,\gamma_p\,\gamma_s\,J}{\gamma_c\left(\gamma_n-\xi_{f_1}\,\gamma_n\right)+\gamma_p\,\gamma_s} \\
s_{2st} = -1 \\
n_{2st} = \left(1+\xi_{c_2}+\dfrac{\xi_{c_2}\,\xi_{f_1}\,\gamma_c\,\gamma_n}{\gamma_c\left(\gamma_n-\xi_{f_1}\,\gamma_n\right)+\gamma_p\,\gamma_s}\right)J
\end{array}\right\}\text{F.P. III} \tag{13}$$

$$\left.\begin{array}{r}
s_{1st} = -1 \\
n_{1st} = \left(1+\xi_{c_1}+\dfrac{\xi_{c_1}\,\xi_{f_2}\,\gamma_c\,\gamma_n}{\gamma_c\left(\gamma_n-\xi_{f_2}\,\gamma_n\right)+\gamma_p\,\gamma_s}\right)J \\
s_{2st} = \dfrac{\xi_{f_2}\,\gamma_c\,\gamma_n}{\gamma_c\left(\gamma_n-\xi_{f_2}\,\gamma_n\right)+\gamma_p\,\gamma_s} \\
n_{2st} = \dfrac{\xi_{f_2}\,\gamma_p\,\gamma_s\,J}{\gamma_c\left(\gamma_n-\xi_{f_2}\,\gamma_n\right)+\gamma_p\,\gamma_s}
\end{array}\right\}\text{F.P. IV} \tag{14}$$

two solutions, in which one laser is turned-on while the other is turned-off.

It is worth noting the existence of a divergence of the photon and carrier densities for the fixed points I, III and IV for a suitable choice of the coupling and feedback strengths. This meaningless fact just represents the necessity of including more nonlinear terms (besides the differential and linear saturation gain terms) in the equations which eventually bound the density of photons when the latter would tend to increases. Consequently, we restrict ourselves to regions in the coupling-feedback parameter space where no divergences occur and our model does not need to be modified to describe accurately the dynamics of the system.

4. STABILITY AND ROUTE TO CHAOS

In the following, we focus our attention in the stability of steady states and limit cycles. This study has been partly carried out analytically and partly using the Matlab package DDE-BIFTOOL[15] which allows the computing, continuation and stability analysis of steady states and periodic solutions of delay differential equations with both constants and state-dependent delays.

For the fixed points, once the system has been linearized around a steady state, an exponential ansatz leads to the conclusion that their stability is governed by the roots of the characteristic equation $det\Delta(\lambda) = 0$ with

$$\mathbf{\Delta}(\lambda) \equiv -\lambda\mathbf{I} + \left.\frac{\partial \mathbf{f}}{\partial \mathbf{x}}\right|_{\mathbf{x_{st}}} + \left.\frac{\partial \mathbf{f}}{\partial \mathbf{x}_{\tau_f}}\right|_{\mathbf{x_{st}}} \exp(-\lambda\tau_{\mathbf{f}}) + \left.\frac{\partial \mathbf{f}}{\partial \mathbf{x}_{\tau_{c1}}}\right|_{\mathbf{x_{st}}} \exp(-\lambda\tau_{\mathbf{c_1}}) + \left.\frac{\partial \mathbf{f}}{\partial \mathbf{x}_{\tau_{c2}}}\right|_{\mathbf{x_{st}}} \exp(-\lambda\tau_{\mathbf{c_2}})$$

where $\mathbf{x} \doteq (s_1, n_1, s_2, n_2)^\dagger$, $\mathbf{f}$ is the flow defined by equations (6-9) and the notation $\mathbf{x}_\tau$ stands for $\mathbf{x}(\mathbf{t}-\tau)$. A fixed point of the system is exponentially stable as time goes to infinity if and only if the associated characteristic equation has no roots with positive real part (i.e., in the right half-plane of the complex plane). For this reason, the pure imaginary eigenvalues have an special interest indicating the regions where a Hopf bifurcation can take place.

The Floquet multipliers of the limit cycles that born after a Hopf bifurcation are also studied by continuing the branch of periodic solutions when some parameter is varied. The type of instabilities ocurring is then predicted observing the way in which the different Floquet multipliers leave the unit circle.

Now, we split our analysis in two important configurations. First, we consider the situation where both lasers are not subject to optoelectronic feedback but are mutually coupled. After that, we analyze the scheme in which both lasers operate with its own feedback loop besides the bidirectional coupling.

4.1. Case I: Bidirectional coupling without feedback

For this case (where $\xi_{f_1} = \xi_{f_2} = 0$ and $\xi_{c_1} = \xi_{c_2} = \xi_c$) the computation of the characteristic equations yields to different situations for each one of the fixed points.

4.1.1. Fixed Point I

Under the conditions we are imposing, the fixed point defined by equation (11) becomes a symmetric one ($s_{1st} = s_{2st} = s$, $n_{1st} = n_{2st} = n$) and the associated characteristic equation reads

$$\begin{aligned} det\Delta(\lambda) &= -\left(\exp\left(-\lambda\frac{\tau_{c_1}+\tau_{c_2}}{2}\right)\xi_c\,\gamma_c\,\gamma_n\,(1+s)\right)^2 \\ &+ \left(\frac{\gamma_s\,J\,(\gamma_p\,(\gamma_s+\lambda)\,(1+2\,s)+\lambda\,(\gamma_n+\gamma_s+\lambda+\gamma_n\,s))+\gamma_c\,\gamma_n\,(-\lambda\,n+\gamma_s\,(J-n+J\,s))}{\gamma_s\,J}\right)^2 \\ &= 0 \end{aligned} \tag{15}$$

An important point to note here, is that since the delay times (τ_{c_1} and τ_{c_2}) appear in the above equation only through their sum, the actual value of each of them is not important provided their sum remains constant. Defining $\tau_c \equiv (\tau_{c_1} + \tau_{c_2})/2$ and separating in real and imaginary parts both sides of equation (15) after the substitution $\lambda = i\omega$ has been inserted, the delay time can be easily eliminated, reducing the characteristic equation to a biquadratic one

$$\omega^4 + b\,\omega^2 + c = 0 \tag{16}$$

where the coefficients b and c are given by

$$
\begin{aligned}
b &= \left(\frac{\gamma_c\,\gamma_n\,n}{\gamma_s\,J}\right)^2 + \left(\gamma_s{}^2 + \gamma_n{}^2\,(1+s)^2 + (\gamma_p + 2\,\gamma_p\,s)^2 + 2\,\gamma_n\,(1+s)\,(\gamma_p + \gamma_s + 2\,\gamma_p\,s)\right) \\
&- \frac{2\,\gamma_c\,\gamma_n}{\gamma_s\,J}\,(\gamma_s\,J\,(1+s) + n\,(\gamma_n + \gamma_p + \gamma_n\,s + 2\,\gamma_p\,s)) \qquad (17) \\
c &= \frac{(\gamma_p\,\gamma_s\,J\,(1+2\,s) + \gamma_c\,\gamma_n\,(J - n + J\,s))^2 - (J\,\xi_c\,\gamma_c\,\gamma_n\,(1+s))^2}{J^2} \qquad (18)
\end{aligned}
$$

The solutions of (16) are

$$
\omega = \pm\frac{1}{\sqrt{2}}\sqrt{-b \pm \sqrt{b^2 - 4c}} \qquad (19)
$$

Then, once the values of ω have been obtained, the critical delay time is given by

$$
\tau_c(\omega) = \frac{1}{\omega}\arctan\left[-\left(\frac{\omega\,(\gamma_s\,J\,(\gamma_p + \gamma_s + 2\,\gamma_p\,s) + \gamma_n\,(-\gamma_c\,n + \gamma_s\,J\,(1+s)))}{\gamma_s\,(\gamma_c\,\gamma_n\,(J - n + J\,s) + J\,(-\omega^2 + \gamma_p\,(\gamma_s + 2\,\gamma_s\,s)))}\right)\right] \qquad (20)
$$

Due to the periodicity in τ_c of the term $\exp(-2i\omega\tau)$ in (15) when the condition of pure imaginary eigenvalue has been imposed, it is evident that if τ_c is a critical delay time, then any delay of the form $\tau = \tau_c + n\pi/\omega$ $\forall n \in \mathbb{Z}$, will be also a critical delay time.

From the inspection of equation (19) it is observed that a necessary and sufficient condition for the existence of a critical delay is that $-b \pm \sqrt{b^2 - 4c}$ is a real and positive quantity. Then, since the coefficients b and c only depend on the current injection J and coupling strength ξ_c, once we have fixed the internal parameters we can obtain the regions in the coupling-current plane where at least one real solution for ω exists and consequently there is a critical delay time associated to it. Since the expression for τ_c is invariant under the transformation $\omega \mapsto -\omega$ we only distinguish two branches of solutions depending on the sign that we choose inside the square root (ω_1 and ω_2 for the positive and negative signs, respectively). Therefore, besides the necessary condition $D \equiv b^2 - 4c \geq 0$, in Table 1 we collect the conditions on the coefficients b and c (actually they depend only on the sign of b and c) for the existence of real values for ω_1 and ω_2.

$D \geq 0$	$c > 0$	$c = 0$	$c < 0$
$b > 0$	$\omega_1,\,\omega_2 \notin \mathbb{R}$	$\omega_1 = 0,\,\omega_2 \notin \mathbb{R}$	$\omega_1 \in \mathbb{R},\,\omega_2 \notin \mathbb{R}$
$b < 0$	$\omega_1,\,\omega_2 \in \mathbb{R}$	$\omega_1 = 0,\,\omega_2 \in \mathbb{R}$	$\omega_1 \in \mathbb{R},\,\omega_2 \notin \mathbb{R}$

Table 1: Classification of the real solutions for the characteristic equation.

Note that the case $b = 0$ has not been considered since it violates the condition $D \geq 0$ unless $c = 0$ in which case both ω_1 and ω_2 are equal to zero. In Figure 2 we show the different regions of the coupling-current plane according to the former table. The internal parameters of the lasers used in this figure and in the following numerical simulations are given by $\gamma_c = 0.24 \times 10^{11}$ s^{-1}, $\gamma_s = 1.458 \times 10^9$ s^{-1} and $\gamma_n = 3J \times 10^9$ s^{-1}.

As it can be seen, the size of the different regions in this coupling-current plane are quite sensitive to the saturation parameter. An increase of the latter produces a reduction in the ranges of pump current and coupling coefficients where a loss of stability can appear for a suitable choice of the delay time. Then, as it is expected the saturation becomes an important parameter that tends to stabilize the dynamics of the system.

In order to incorporate the effect of the delay time, we fix the bias current to a value $J = 1/3$ and assume a gain saturation of $\gamma_p = 1.2 \times 10^{-3}$ ps^{-1}. From Figure 2a it is obtained that the range for the coupling strength

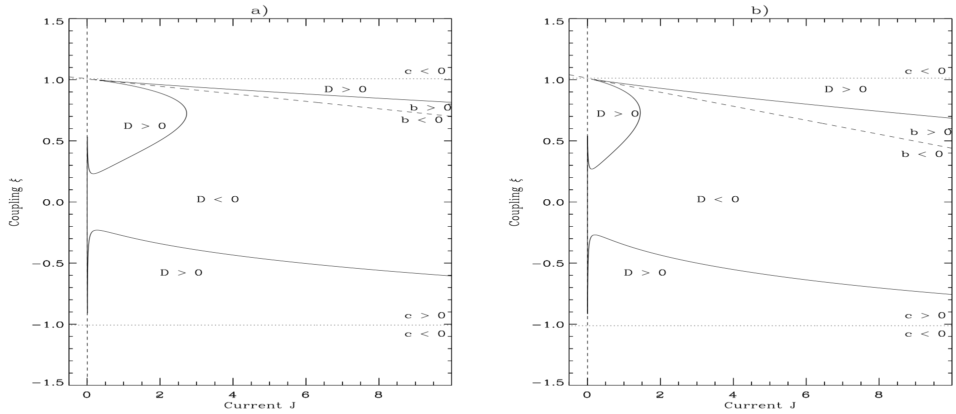

Figure 2. Partition of the coupling-current plane according to the sign of D, b and c for values of the gain saturation coefficient a) $\gamma_p = 3.6J \times 10^9\ \mathrm{s}^{-1}$ and b) $\gamma_p = 6J \times 10^9\ \mathrm{s}^{-1}$. Solid, dashed and dotted lines represent the zero-level contours for D, b and c, respectively.

which can lead to an instability is $\xi_c \in \{(-\infty, -0.23], [0.24, 0.99]\}$. Consequently, for this range we compute the critical delay times associated to the two branches of (19), bearing in mind the periodicity in τ_c that we have previously mentioned. The results are depicted in Figure 3 where the critical delay curves are plotted as function of the coupling strength for both ω_1 and ω_2 eigenfrequencies.

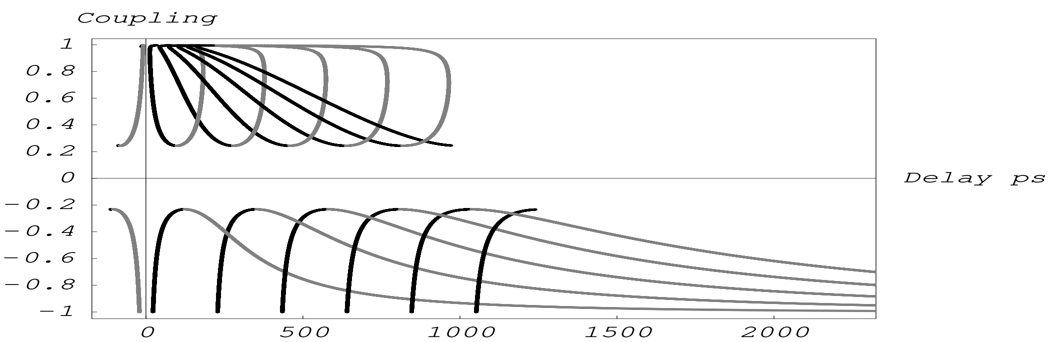

Figure 3. Plot in the coupling-delay plane of the regions where some eigenvalue takes its real part equal to zero. The curves $\tau(\omega_{1,2}) = \tau_c(\omega_{1,2}) + n\pi/\omega_{1,2}$ with $n = 0, 1, 2, 3, 4$ and 5 have been plotted. Black and grey tonalities distinguishes between the sequences associated to ω_1 and ω_2, respectively.

Despite of the fact that crossing one of these lines the real part of one eigenvalues changes its sign, this still do not determine the stable (unstable) region for this fixed point. In fact the stability region is determined from the direction of the transition and the number of eigenvalues with positive real part. This means that the stability boundary is formed by the critical lines at which the transition of the eigenvalue is from negative to positive real parts and do not exist eigenvalues in the positive real part half-plane. To compute the direction of the transition of the eigenvalue when crossing the imaginary axis it is necessary to evaluate their derivative at that point. Implicit derivation of equation (15) with respect to τ_c leads to the expression

$$\frac{d\lambda}{d\tau_c} = \frac{-\lambda \exp(-2\lambda\tau_c)}{g(\lambda)\frac{\partial g}{\partial \lambda} + \tau_c \exp(-2\lambda\tau_c)} \tag{21}$$

where $g(\lambda)$ denotes the function

$$g(\lambda) = \frac{\gamma_s\, J\, \left(\gamma_p\, \left(\gamma_s + \lambda\right)\, \left(1 + 2\, s\right) + \lambda\, \left(\gamma_n + \gamma_s + \lambda + \gamma_n\, s\right)\right) + \gamma_c\, \gamma_n\, \left(-\lambda\, n + \gamma_s\, \left(J - n + J\, s\right)\right)}{\xi_c\, \gamma_c\, \gamma_n\, \left(1 + s\right)\, \gamma_s\, J}$$

We have numerically evaluated $dRe(\lambda)/d\tau|_{\lambda=i\omega_{1,2}}$ from equation (21) as function of n (the periodicity order in τ_c) for several coupling constants. The results are plotted in Figure 4.

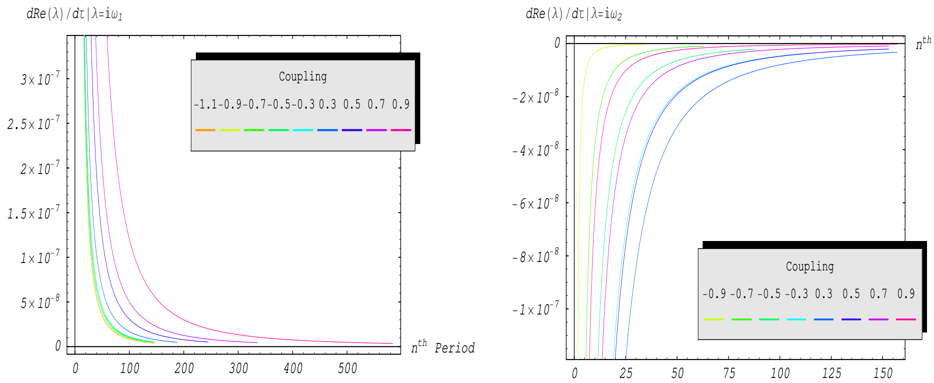

Figure 4: $dRe(\lambda)/d\tau|_{\lambda=i\omega_{1,2}}$ as function of the period order n for several coupling strengths.

Since $dRe(\lambda)/d\tau|_{\lambda=i\omega_1} > 0$ and $dRe(\lambda)/d\tau|_{\lambda=i\omega_2} < 0$, it indicates that destabilizations of eigenvalues occur at the critical delay lines associated to the eigenfrecuency ω_1 while stabilizations occur at the associated to ω_2. From Figure 4, it can be also deduced that the "velocity" at which the eigenvalues are crossing the imaginary axis is a monotically decreasing function of the period order. Since $\omega_1 > \omega_2$ (and consequently $2\pi/\omega_1 < 2\pi/\omega_2$), the rate at which the eigenvalues become unstable at ω_1 is greater than the rate they become stable at ω_2 what indicates that an arbitrary number of unstable eigenvalues can be achieved for delay values long enough. This fact also assures the absence of stability islands inside the external borders of the curves plotted in Figure 3. At this point, we are now able to construct the stability diagram for F.P.I that is shown in Figure 5.

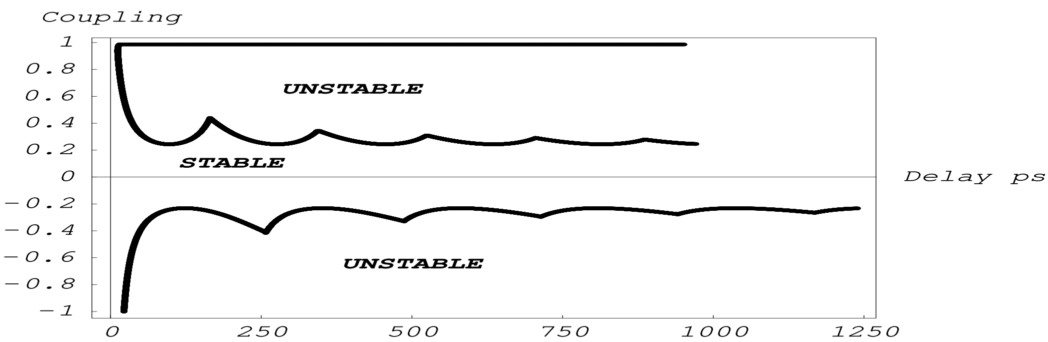

Figure 5. Stability diagram for the F.P. I in the coupling-delay plane obtained from margins of the critical lines in Figure 3.

At the intersection points of the critical lines corresponding to different eigenfrequencies a Hopf-Inverse Hopf codimension two bifurcation takes place with the simultaneous crossing of two pairs of complex conjugate eigenvalues to opposite regions in the complex plane as it can be observed in Figure 6 where we plot the rightmost eigenvalues.

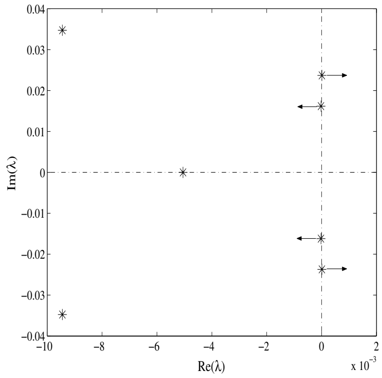

Figure 6. Rightmost roots of the characteristic equation at the Hopf-Inverse Hopf bifurcation located at $\xi_c = 0.43, \tau_c=$ 164 ps in the coupling-delay parameter space. The arrows indicate the direction of the transition.

4.1.2. Fixed Point II

For this steady state in which both lasers do not emit light, the resultant characteristic equation have as a solution $\lambda = (\gamma_c\gamma_n + \gamma_p\gamma_s)/(\gamma_s)$ and takes the zero value when $J = 0$ (i.e. at the threshold pump as it is expected).

4.1.3. Fixed Point III and IV

The symmetry of these two fixed points allows the simultaneous study of both of them. In this case the computation of the characteristic equation leads to the following four eigenvalues

$$\lambda_1 = -\gamma_s \tag{22}$$

$$\lambda_2 = \frac{\gamma_c\,\gamma_n + \xi_c\,\gamma_c\,\gamma_n + \gamma_p\,\gamma_s}{\gamma_s} \tag{23}$$

$$\lambda_{3,4} = \frac{-\gamma_n - \gamma_p - \gamma_s \pm \sqrt{(\gamma_n + \gamma_p + \gamma_s)^2 - 4\,(\gamma_c\,\gamma_n + \gamma_p\,\gamma_s)}}{2} \tag{24}$$

Evaluating the real part of these solutions, it is observed that only the second one can take its real part to zero and it occurs at a coupling strength of $\xi_c = -1 - \gamma_p\gamma_s/\gamma_c\gamma_n$. For values of the coupling more negative than this, F.P.III and F.P.IV become from saddles to stable nodes. This occurs when the effective current (this is the bias current plus the current coming from the coupling $J_{eff} = J + \xi_c(1+s)J$) injected in one laser decreases below the threshold pump.

4.1.4. Limit Cycles and Chaos

In this section we analyze the stability of the limit cycles that born after a given Hopf bifurcation, which provide an appropiate understanding of the route to chaos followed by the system. Figure 7 shows a typical stability diagram for a pair of limit cycles.

In the direction of decreasing the delay, after a subcritical Hopf bifurcation takes place (at the point E, where an eigenvalue becomes unstable), the limit cycle undergoes a stabilizing fold bifurcation at the point B, followed by a Neimark-Sacker bifurcation indicated by the destabilization of a pair of complex conjugate Floquet multipliers at the point A. Further decreasing the delay, a torus breakdown is numerically observed leading to a full developed chaotic behaviour. However, for shorter delays, a sudden disappearance of the chaotic attractor is probably induced by a boundary crisis when the unstable limit cycle of the first periodic solution and the chaotic attractor generated by the second one collide at the point C. Eventually, the amplitude of the periodic solution decreases

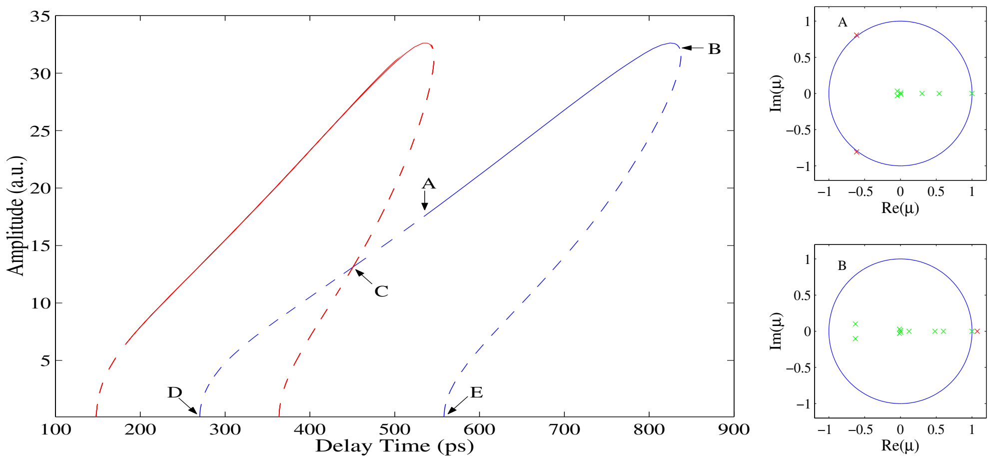

Figure 7. Stability diagram of two periodic solutions as function of the time delay together the Floquet multipliers evaluated at the points A and B. For this calculation the coupling strength has been fixed to $\xi_c = 0.5$.

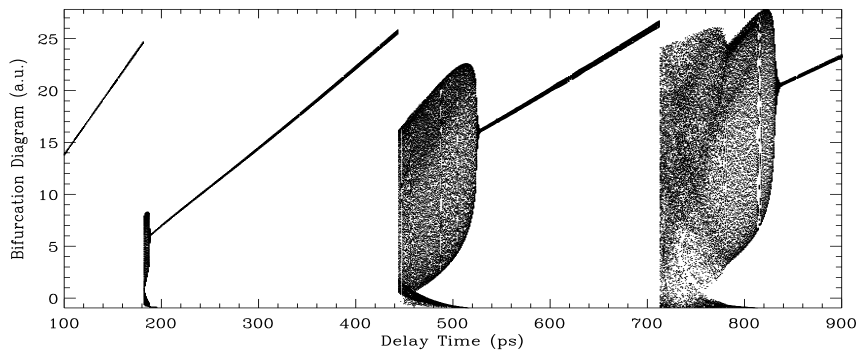

Figure 8: Bifurcation diagram varying the time delay from 100 ps to 900 ps.

to zero at the point D where some eigenvalue is stabilized. The corresponding bifurcation diagram for the range of delays considered before is shown in Figure 8.

The features of the bifurcation diagram coincide with the expected from the above-mentioned analysis taken into account that for this range there are three pairs of limit cycles that interact in the same way than the unique pair we have previously considered. These three pairs generates three different regions of full developed chaos observed in Figure 8. For larger delays the regions of chaotic behaviour overlap producing a continuous region where chaos exists.

4.2. Case II: Bidirectional coupling with feedback

We consider now the case in which both lasers have the same delay time in their feedback loops (ie., $\tau_{f_1} = \tau_{f_2} = \tau_f$). Then, when both lasers are decoupled each one can operate as a self-pulsating oscillator due to the feedback loop, for an appropiate selection of the feedback strength and time delay. In this regime one can observe the phenomenon of the oscillation death or quenching by which the coupling between two oscillators induces an amplitude death of the limit cycles through a collapse to the zero amplitude state. When delay is not present in the coupling term, a large dispersion or detuning in the natural frequencies of the oscillators and a large coupling value are needed to observe this phenomenon besides the requirement that the coupling must be of a diffusive type. Nevertheless, surprisingly these restrictions dissapear when a delay is taken into account in the coupling term. For instance, one can now observe the quenching of two identical oscillators, a forbidden situation for the case of no delay due to the necessity of maintain a detuning between the oscillators frequencies. This "death by delay" can be predicted for our system by looking at the stabilization of the largest eigenvalue as function of the time delay in the coupling. For instance, for the parameter values $\xi_f = -0.3$ and $\tau_f = 210$ ps each laser is a self-pulsating oscillator when they are decoupled. If we couple them with a strength as small as $\xi_c = -0.05$ and we do not consider a delay time in the coupling, they still continue oscillating. However, as it can be seen in Figure 9, where we plot the two largest eigenvalues of the system, as soon as we allow for a delay time in the coupling several death islands appear, indicating the cease of any oscillation in the system.

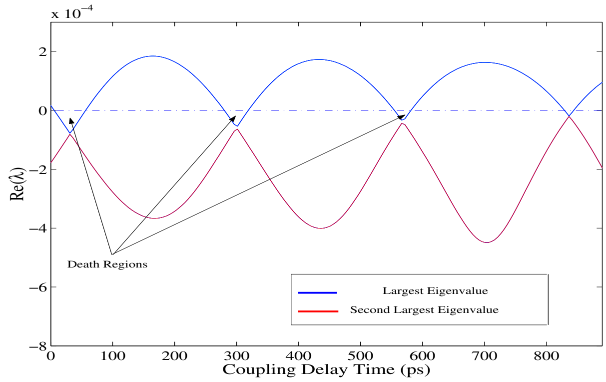

Figure 9: Two largest eigenvalues of the system as function of the delay coupling time.

Altough the parameter regions for which this phenomenon occurs are not very large, the values chosen in the former example by no means constitute an exceptional example. The main difficult in trying to observe this effect experimentally is related to the smallness of the delay times involved in. An all-optical configuration of a similar scheme like the incoherent optical coupling and feedback should allow for the observation of the phenomenon avoiding the limitations introduced by the electronic components of the present case.

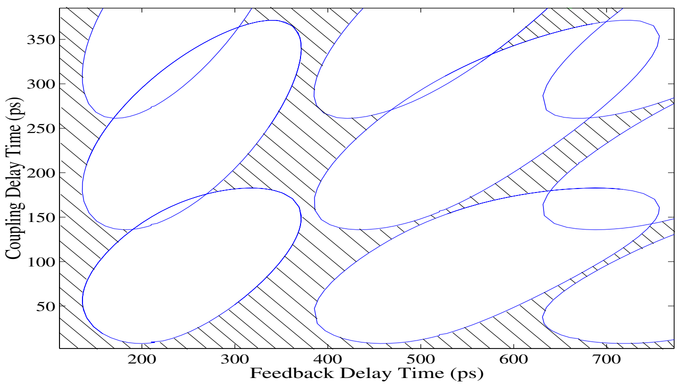

Figure 10: Stability diagram in the coupling-feedback delay times parameter space.

With respect to the stability and route to chaos in this configuration, analytical computations are hopeless. However, numerical results suggest that when the delay coupling time or the delay feedback time are varied, the route to chaos is similar to the case when no feedback is present (i.e. a quasiperiodic route to chaos with crisis events). We can also construct the stability diagram by computing the regions where pure imaginary eigenvalues occur in the coupling-feedback delay times plane. The results are given in Figure 10, where the diagonal grid indicates the stable region once we have fixed the parameters to be $\xi_c = 0.25$ and $\xi_f = 0.25$.

5. CONCLUSIONS AND FUTURE DIRECTIONS

We have studied the dynamics of two mutually optoelectronic coupled semiconductor lasers subject or not to optoelectronic feedback, predicting the route to chaos of the system as well as the observation of the amplitude death when each laser is operating as a self-sustained oscillator. Future work concern to the experimental observation of some of the dynamical regimes predicted for the system and the study of the lagged solutions between both lasers.

ACKNOWLEDGMENTS

R. V. would like to acknowledge Emilio Hernández-García, Pere Colet and Manuel Matías for fruitful dicussions. The authors acknowledge financial support from the Ministerio de Ciencia y Tecnología (Spain) and FEDER (Project Nos. BFM2000-1108, BFM2001-0341, BFM20001-2159, and BFM2002-04369) and from the EC project IST-2000-29683 OCCULT.

REFERENCES

1. J. D. Farmer, "Chaotic attractors of an infinite-dimensional system," *Physica D* **4**, p. 366, 1982.
2. D. V. Ramana, A. Sen, and G. L. Johnston, "Time delay induced death in coupled limit cycle oscillators," *Phys. Rev. Lett.* **80**, p. 5109, 1998.
3. R. Herrero, M. Figueras, J. Rius, F. Pi, and G. Orriols, "Experimental observation of the amplitude death effect in two coupled nonlinear oscillators," *Phys. Rev. Lett.* **84**, p. 5312, 2000.
4. A. Takamatsu, T. Fujii, and I. Endo, "Time delay effect in a living coupled oscillator system with the plasmodium of physarum polycephalum," *Phys. Rev. Lett.* **85**, p. 2026, 2000.
5. D. V. Ramana, A. Sen, and G. L. Johnston, "Experimental evidence of time-delay-induced death in coupled limit-cycle oscillators," *Phys. Rev. Lett.* **85**, p. 3381, 2000.
6. G. Giacomelli, M. Calzavara, and F. Arecchi, "Instabilities in a semiconductor laser with delayed optoelectronic feedback," *Optics Comm.* **74**, p. 97, 1989.
7. C. Lee and S. Shin, "Self-pulsing, spectral bistability, and chaos in a semiconductor lasers diode with optoelectronic feedback," *Appl. Phys. Lett.* **62**, p. 922, 1992.
8. N. A. Loiko and A. M. Samson, "Possible regimes of generation of a semiconductor laser with a delayed optoelectric feedback," *Optics Comm.* **93**, p. 66, 1992.
9. E. V. Grigorieva, H. Haken, and S. A. Kaschenko, "Theory of quasiperiodicity in model of lasers with delayed optoelectronic feedback," *Optics Comm.* **165**, p. 279, 1999.
10. S. Tang and J. M. Liu, "Chaotic pulsing and quasi-periodic route to chaos in a semiconductor laser with delayed opto-electronic feedback," *IEEE J. of Quantum Electron.* **37**, p. 329, 2001.
11. H. D. I. Abarbanel, M. B. Kennel, L. Illing, S. Tang, H. F. Chen, and J. M. Liu, "Synchronization and communication using semiconductor lasers with optoelectronic feedback," *IEEE J. of Quantum Electron.* **37**, p. 1301, 2001.
12. S. Tang and J. M. Liu, "Synchronization of high-frequency chaotic optical pulses," *Optics Lett.* **26**, p. 596, 2001.
13. H. T., I. Fischer, W. Elssser, J. Mulet, and C. Mirasso, "Chaos synchronization ans spontaneous symmetry-breaking in symmetrically delay-coupled semiconductor lasers," *Phys. Rev. Lett.* **86**, p. 795, 2001.
14. J. Mulet, C. Masoller, and M. C. R., "Modeling bidirectionally coupled single-mode semiconductor lasers," *Phys. Rev. A* **65**, p. 063815, 2002.
15. K. Engelborghs, T. Luzyanina, and G. Samaey, "Dde-biftool v. 2.00 user manual: a matlab package for bifurcation analysis of delay differential equations.," *Technical Report TW-330, Department of Computer Science, K. U. Leuven, Leuven, Belgium* , 2001.